Surveys in Geophysics (2005) 26:701–731
DOI: 10.1007/s10712-005-1831-2
© Springer 2005

ELECTRICAL STRUCTURE IN MARINE TECTONIC SETTINGS

KIYOSHI BABA[1,2],
[1]*Institute for Research on Earth Evolution, Japan Agency for Marine-Earth Science and Technology, 2-15 Natsushima, Yokosuka, Kanagawa, 237-0061, Japan;*
[2]*Earthquake Research Institute, University of Tokyo, 1-1-1, Yayoi, Bunkyo-ku, Tokyo, 113-0032, Japan; E-mail: kbaba@eri.u-tokyo.ac.jp*

(Received 10 December 2004; accepted 23 May 2005)

Abstract. This review paper presents recent research on electrical conductivity structure in various marine tectonic settings. In at least three areas, marine electromagnetic studies for structural exploration have increasingly progressed: (1) data accumulations, (2) technical advances both for hardware and software, and (3) interpretations based on multidisciplinary approaches. The mid-ocean ridge system is the best-studied tectonic setting. Recent works have revealed evidence of conductive zones of hydrothermal circulation and axial magma chambers in the crust and partial melt zones of the mid-ocean ridge basalt source in the mantle. The role of water or dissolved hydrogen and its redistribution at mid-ocean ridges is emphasized for the conductivity pattern of the oceanic lithosphere and asthenosphere. Regions of mantle upwelling (hotspot or plume) and downwelling (subducting slab) are attracting attention. Evidence of heterogeneity exists not only in the crust and the upper mantle, but also in the mantle transition zone. Electrical conductive zones frequently overlap seismic low-velocity zones, but discrepancies are also apparent. Some studies have compared conductivity models with the results of seismic and other studies to investigate the physical properties or processes. A new laboratory-based conductivity model for matured oceanic lithosphere and asthenosphere is proposed. It takes account of both the water distribution in the mantle as well as the thermal structure. It explains observed conductivity patterns in the depth range of 60–200 km.

Keywords: controlled-source electromagnetics, electrical conductivity, magnetotellurics, marine tectonic settings

1. Introduction

This review is intended to cover the main results on marine electromagnetic (EM) studies since Palshin (1996), with particular emphasis on electrical conductivity and resistivity structures in various marine tectonic settings. Heinson (1999) presented a more recent review emphasizing the structure of both the oceanic and continental lithosphere and asthenosphere. Motional induction by ocean currents is another interesting target of active study by several groups (e.g., Flosadóttir et al., 1997; Fujii and Utada, 2000; Lilley et al., 2001, 2004). However, that subject is beyond the scope of this review. The papers cited should be used for reference.

Marine EM studies for structural exploration have progressed rapidly during the last decade. At least three reasons for this progress exist: (1) data accumulation, (2) technical advances, and (3) interpretations based on multidisciplinary approaches.

Data sets have been accumulated from various tectonic settings. The most actively studied setting is the mid-ocean ridge system. Subduction zones and back-arc basins have also been increasingly investigated. Aside from those, a few experiments have been undertaken in mantle upwelling regions, normal oceanic basins, and passive continental margins. Now standard exploration methods to produce an image of the conductivity structure beneath the seafloor are magnetotellurics (MT), geomagnetic depth sounding (GDS), and controlled-source methods: time and frequency domain controlled-source electromagnetic (CSEM) systems and magnetometric resistivity (MMR) soundings. An overview of marine EM techniques is given by Chave et al. (1991). The exploration range using such methods extends from the shallow crust to the deep upper mantle. Long-distance and long-term voltage difference data measured by submarine cables have also been accumulated. Use of data from such cables and magnetic observatories for MT and GDS allows probing of the submarine deep mantle structure on a super-regional or semi-global scale.

Technical advances in both hardware and software support the progress of marine EM studies. Hardware improvements include the development of new instruments to improve the depth range of conventional surveys. Software advances comprise new modeling and inversion techniques, supported by steadily improving computer performance. Two-dimensional (2D) analysis using regularized inversion has become a standard approach in many studies. Even three-dimensional (3D) inversion methods have been developed and applied. Some inversion programs that were designed originally for land-based data have been adapted for marine applications. Some newly developed methods exist to treat typical problems for seafloor observations, such as incorporation of deep-towed active sources and seafloor topography into the model.

The interpretation of the obtained conductivity or resistivity models has become more sophisticated because of improvement of data quality and density, and most notably because of the increasing trend towards multidisciplinary studies. Comparison of the conductivity structure with other observations, experimental studies, and modeling studies has helped to distinguish factors that determine physical properties and processes. Comparisons of electrical conductivity structure with seismic velocity structure are obtainable from many recent publications (e.g., Evans et al., 2005; Fukao et al., 2004; Key and Constable, 2002; MacGregor et al., 2001).

In the following sections, recent technical advances are reviewed first. Then, some case studies from different tectonic settings – the mid-ocean ridge system, mantle upwelling, and downwelling regions – are discussed. Finally, a new laboratory-based conductivity model for oceanic lithosphere and

asthenosphere is introduced. It is helpful for interpretation of seafloor MT observations.

2. Technical advancements

2.1. Instrumentation

The respective developmental histories of at least two novel instruments for seafloor EM exploration are available among recent studies. Constable et al. (1998) describe a newly developed broadband MT instrument for exploration of shallow structures. The seafloor MT method has traditionally been used in the period range of $10^3 - 10^5$ s because the MT fields at shorter periods are attenuated by the presence of conductive seawater. Because of its range, the MT method is capable of probing the upper mantle structure in a depth range of ~20 to ~400 km, whereas controlled-source methods have been utilized to investigate the shallow conductivity structure in a depth range between tens of meters and tens of kilometers using an artificial transmitter source. The new instrument is equipped with induction coil sensors and AC-coupled electric field amplifiers and allows measurements in the range of 1–1000 s, which is suitable to detect targets in the crust and shallow mantle. Practical use of these types of instruments is reported by Key and Constable (2002) and Goto (2003) among others.

A new type of seafloor electromagnetic station (SFEMS) has been developed for long-term measurement of EM fields on the seafloor with an accuracy that is equivalent to land observatories (Toh et al., 1998, 2001). For this purpose, the SFEMS is equipped with an Overhauser absolute magnetic sensor and a fiber optical gyro aside from an MT variograph (three-component fluxgate magnetometer, electric dipoles, and tilt meters). The SFEMS was developed with the intentions of (1) probing the conductivity structure of the deep Earth using long-term seafloor MT soundings, (2) estimating lower mantle conductivity by detection of geomagnetic secular variations, and (3) understanding the dynamics in the Earth's core by improving the distribution of the existing global EM observation network. The SFEMS was deployed on the seafloor in Northwest Pacific in August (2001), and 718 daytime series data have been recovered since its deployment; those measurements are ongoing (Toh et al., 2004).

2.2. Modeling and inversion techniques

Modeling and inversion techniques have been improved continually along with the ongoing progress in computing technology. 2D inversion has become a standard tool; the availability of sophisticated 3D inversion codes

is anticipated. As data quality and density improve, demand grows for more accurate and reliable determination of the Earth structure in complex terrains. Taking the effect of topography into account is an important aspect of this progress. Accounting for topography is particularly important when data are acquired on the seafloor because the large conductivity contrast between seawater and crust severely distorts both electric and magnetic fields whereas the topographic distortion appears mainly in the electric field on land. Schwalenberg and Edwards (2004) present analytic solutions for the fields perturbed by a 2D sinusoidal topographic interface and demonstrate their effects on the MT response. Although the analytic approach provides solutions for a limited model, it is useful to understand the physics of the distortion process and to check numerical algorithms.

Figure 1 shows the topographic model and the calculated MT response demonstrated by Schwalenberg and Edwards (2004) for interfaces between two media: a land surface and a seafloor. On the seafloor, both the TE and TM mode responses are affected by the topography, whereas only the TM mode apparent resistivity is distorted on land. The TM mode apparent resistivities are distorted in an opposite sense depending on whether the upper medium is more conductive than the lower medium (seafloor) or more resistive (land surface). For the TM mode response, only the apparent resistivities, not the phases, are distorted by topography in both cases. The distortion is independent of the period, indicating that galvanic charge effects are dominant. For the TE mode, however, both the apparent resistivity and phase are distorted on the seafloor and are strongly dependent on the frequency, demonstrating that the effect is rather inductive. This fact complicates the separability of the effects of topographic distortion from seafloor responses in the data analysis. It also eliminates the application of tensor decomposition techniques for galvanic distortion correction (e.g., Groom and Bailey, 1989; Chave and Smith, 1994).

Distorted fields caused by changing topography typically engender large problems in numerical modeling in the period range used for seafloor MT. The reason is that it is difficult to simultaneously resolve the small-scale heterogeneity (relative to the induction scale) that produces the distortion and still include the much larger scale, heterogeneous structure of the underlying mantle, which is of geophysical interest. The thin-sheet approximation (Price, 1949) is frequently used. It conceptually replaces an actual ocean layer with various thicknesses as a result of seafloor topography with a thin sheet of variable conductance (e.g., Heinson and Lilley, 1993; Nolasco et al., 1998; Evans et al., 1999). However, the thin sheet approximation is limited to application to 1D models. Furthermore, it becomes increasingly inaccurate at periods shorter than $\sim$1000 s in the deep ocean because the electromagnetic skin depth becomes comparable to the water depth. Another common

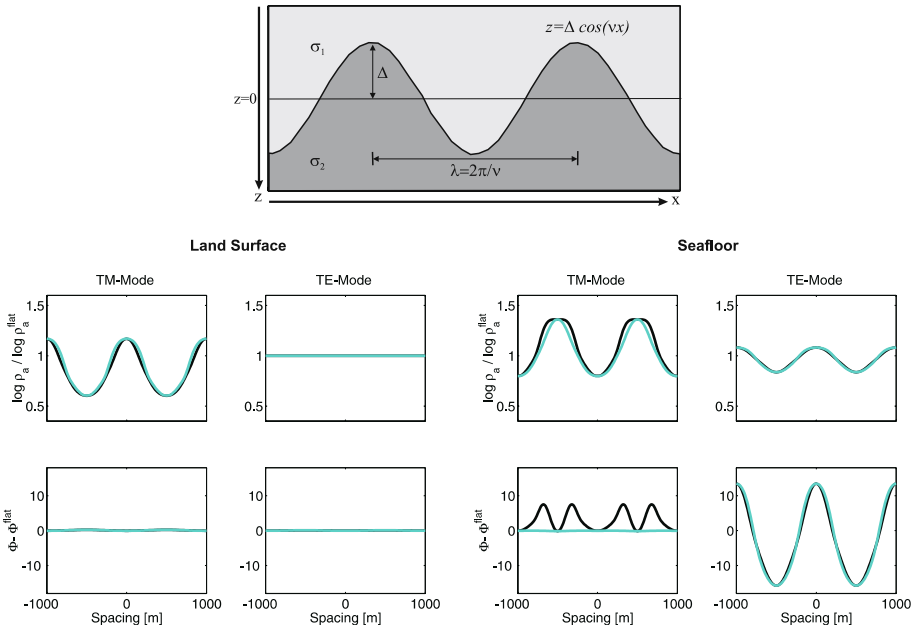

Figure 1. Modeling of the topographic effect using an analytic approach (Schwalenberg and Edwards, 2004). Top: The topographic model. Bottom: Normalized apparent resistivity and phases calculated on a harmonic interface.

approach is to incorporate a simplified 2D topography in the discrete model (e.g., Evans et al., 1999; Constable and Heinson, 2004).

Baba and Seama (2002) recently introduced an effective modeling technique called flattening surface 3D modeling (FS3D), which can incorporate precise 3D topography over an arbitrary subsurface structure without invoking the thin sheet approximation. The FS3D method is based on conversion of 3D changes in the electrical conductivity and magnetic permeability of blocks bounding the flattened seafloor. Consequently, number of vertical grid points is considerably smaller than that used for a full 3D simulation (Figure 2). The topographic problem has been long-standing in marine EM studies. Its solution has been attempted by many authors (e.g., Heinson and Lilley, 1993; Nolasco et al., 1998; Koyama, 2002). Baba and Chave (2005) introduce an analytical method for seafloor MT data that combines the removal of 3D topographic effects with the inversion of the corrected data as follows. The observed MT impedance is first corrected to a flat-lying seafloor datum using the observed bathymetry and FS3D method. The corrected MT response is then inverted in a flat seafloor model space. Because of coupling between the topographic effect and deeper structure, the correction and inversion steps are iterated until their respective changes become small. The method was applied to a real data set (Baba and Chave, 2005; Baba et al., 2004 a).

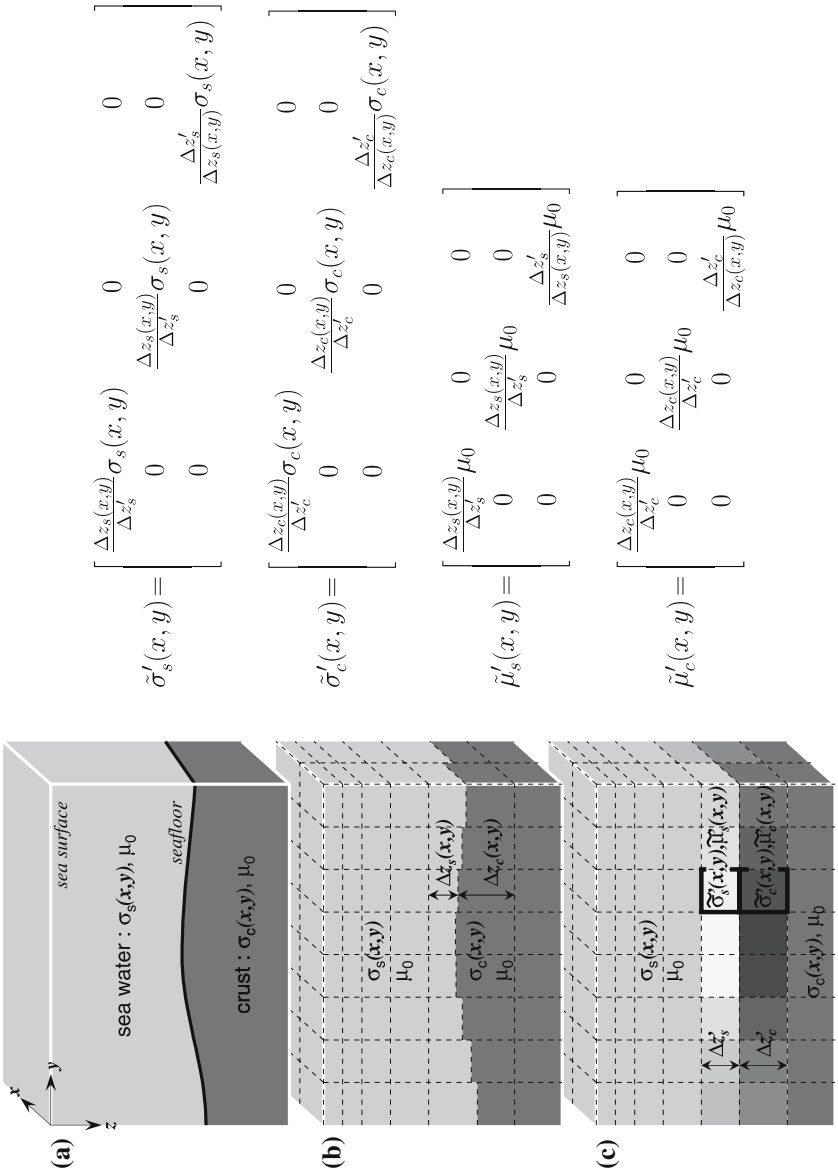

Figure 2. The principle of Baba and Seama (2002)'s FS3D method: (a) the real earth; (b) the earth divided into rectangular blocks, so that topographic change is expressed by variations in the thickness of the blocks at the two layers bounding the seafloor; (c) the FS3D model where the seafloor is flattened and the conductivity and permeability in the two layers are converted to tensors as conductance and permeance in each direction are conserved. The associated equations are provided in the right column.

Numerous 2D MT inversion codes are available (e.g., deGroot-Hedlin and Constable, 1990; Smith and Booker, 1991; Uchida, 1993; Siripunvaraporn and Egbert, 2000; Rodi and Mackie, 2001). Some of these have been modified and applied to seafloor data. One of these modifications accommodates electric and magnetic field observations that are not co-located, for example, because of instrument failure. This modification only slightly affects the TE mode, but it is important for the TM mode because the magnetic field varies according to the position on the seafloor, unlike that on the land surface. The modification was done for the rapid relaxation inversion (RRI) method (Smith and Booker, 1991) in Evans et al. (1999), for the nonlinear conjugate gradient (NLCG) inversion (Rodi and Mackie, 2001), in Chave et al. (2001) and Baba et al. (2004a), and for the inversion method of Uchida (1993) in T. Goto, pers. commun (2004).

Anisotropy is another common problem, particularly when addressing the conductivity structure of the upper mantle. Motivated by the mantle dynamics beneath the East Pacific Rise, Baba et al. (2004a) extended the NLCG inversion by Rodi and Mackie (2001) and incorporated anisotropy into the code. The principle axes of the conductivity tensor are assumed to be in alignment with the 2D regional structure. In other words, only the diagonal terms have non-zero values. The forward solution for the TM mode was modified by incorporating different resistivities in the horizontal and vertical directions, whereas it is identical with the isotropic case for the TE mode. Two regularization terms, one for the model smoothness and the other one for the degree of isotropy, were introduced in the inversion.

For marine CSEM data, regularized one-dimensional (1D) inversion have been state-of-the-art until recently (Evans et al., 1994; Constable and Cox, 1996; MacGregor et al., 1998). MacGregor (1999) describe the development of a 2.5-dimensional (2.5D) regularized inversion scheme for marine CSEM data based on the Occam inversion algorithm (Constable et al., 1987; deGroot-Hedlin and Constable, 1990). Forward calculation is performed using the finite element code of Unsworth et al. (1993). The problem is termed 2.5D because the CSEM source is a point horizontal electric dipole.It generates fields that vary in three dimensions. The 2.5D inversion method was applied to data collected from the Valu Fa Ridge, Lau Basin (MacGregor et al., 2001).

Koyama (2002) developed a 3D regularized inversion algorithm based on a spherical coordinate system to investigate the semi-global scale structure of the mid-mantle. The algorithm is based on an integral equation approach for the forward problem. It makes use of the hybrid method of the quasi-Newton and the steepest descent methods for the inversion problem. The 3D inversion was applied to a data set using trans-Pacific submarine cables and magnetic observatory data (Koyama, 2002; Fukao et al., 2004).

3. Mid-ocean Ridges

Mid-ocean ridge systems, including back-arc spreading centers, have been studied using various geophysical and geochemical approaches, as well as experimental and numerical modeling approaches. Recently, marine EM experiments were carried out in the East Pacific Rise, the Juan de Fuca Ridge, the Gulf of Aden, the Valu Fa Ridge, and the Mariana Trough. Melt generation and migration processes, crustal formation at the axial magma chamber, and hydrothermal circulations have been investigated through the conductivity structure of the crust and mantle.

3.1. Melt generation and migration processes in the upper mantle

At mid-ocean ridges, upwelling mantle partially melts as a result of pressure release. The melt is the source of mid-ocean ridge basalts (MORB). The melt-generating processes have been revealed considerably through the mantle electromagnetic and tomography (MELT) experiment (The MELT Seismic Team, 1998; Evans et al., 1999) in the Southern East Pacific Rise (SEPR) at 17°S, where the Pacific and Nazca plates are spreading rapidly at the full rate of 145 mm/year. The MT experiment was carried out deploying 47 seafloor instruments from four countries at 32 stations on two lines crossing the SEPR during 1996–1997. Evans et al. (1999) reported the first results indicating a broad but asymmetric conductive zone beneath the SEPR (Figure 3c). Subsequently, Baba et al. (2004a) reanalyzed the data using precise topographic effect correction and 2D anisotropic inversion, as mentioned in the previous section. Figure 3a and b respectively show the isotropic and anisotropic models. Anisotropy is considered for the three resistivities in the along-ridge, across-ridge (plate spreading), and vertical directions. The anisotropic model provides a slightly better fit to the data for a given level of model smoothness. Furthermore, it is more consistent with other geophysical and laboratory data. For all the directions, the anisotropic model shows a resistive uppermost 60 km of mantle with a flat boundary across most of the survey region, except in the vicinity of the ridge axis. Off-axis, and to the east of the ridge (to the right of the panel), the mantle is more conductive in the direction of plate spreading ($\rho_{yy} < \rho_{xx}$) at depths of 60–120 km.

Baba et al. (2004a) and Evans et al. (2005) argue that a scenario explaining the conductivity pattern is given by Hirth and Kohlstedt (1996) who proposed that the redistribution of water caused by partial melting controls the rheology of the oceanic lithosphere and asthenosphere. The upwelling mantle beneath the ridge axis starts to melt when it passes the depth of the wet solidus (~115 km). The melt fraction is very limited between ~114 and 60–70 km, where it passes the dry solidus. The melting process is enhanced

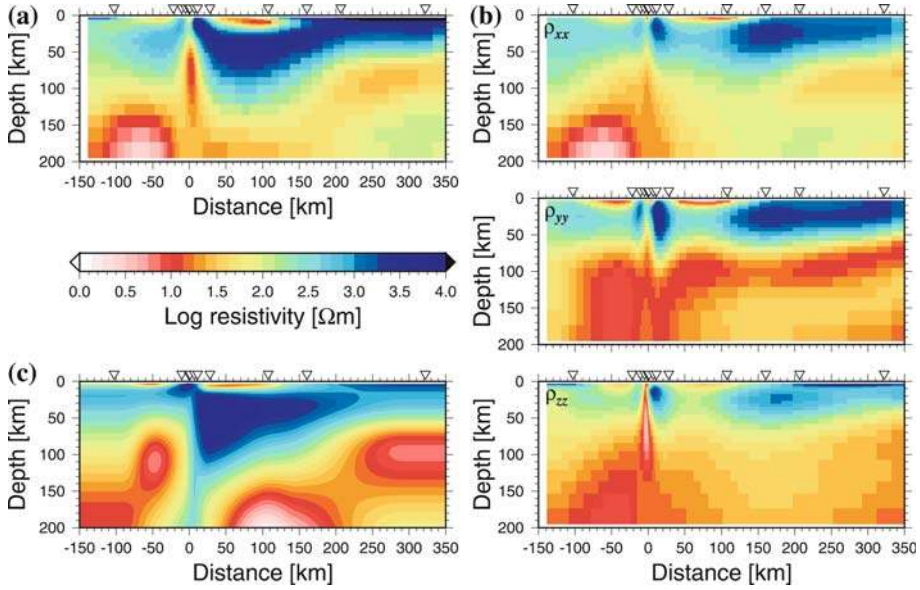

Figure 3. 2D mantle resistivity models in the MELT area (Baba et al., 2004a): (a) and (b) respectively show isotropic and anisotropic models obtained using the anisotropic inversion; (c) depicts the model obtained using RRI by Evans (1999). For (b), the top panel shows resistivity in the along-ridge direction. The middle and bottom panels respectively show resistivities in the spreading direction and the vertical direction. The rise axis is located at 0 km on the horizontal axis; triangles indicate the MT site locations used for respective inversions.

above the dry solidus. Water is extracted preferentially from olivine into melt. As a result, wet mantle material with low viscosity flows to both sides of the rise axis below the dry solidus, whereas dry, and therefore highly viscous, mantle material flows above. This model predicts a boundary between a dry and a wet mantle at around 60 km, which agrees well with the anisotropic conductivity model. The resistive–conductive boundary in the anisotropic model is not a thermal feature. Electrical anisotropy is much greater within the conductive region than in the resistive overlying layer. The conductivity of olivine is enhanced by the diffusion of hydrogen (Karato, 1990). It is much higher in the [100] (*a*-axis) direction because of the anisotropy of the diffusion (Kohlstedt and Mackwell, 1998). The alignment of the olivine *a*-axis to the shear stress direction is observed in ophiolites. For that reason, it is considered that the olivine *a*-axis aligns with the spreading direction. Consequently, the anisotropic conductivity structure model further supports the dry–wet transition model. Seismic data collected by the MELT experiment also support the alignment of olivine *a*-axis in terms of S-wave splitting, where the direction of fast S-wave polarization is aligned parallel to the spreading direction (Wolfe and Solomon, 1998).

Indications for a transition zone from resistive to conductive material at ~60 km depth can also be seen in the models derived from more recent MT experiments in the Mariana Trough (Baba et al., 2004b) and in the Gulf of Aden (Toh, 2003). The Mariana Trough is a back arc basin that is now opening with a slow spreading rate (the western half rate is ~15 mm/year). The Gulf of Aden is separating the African and the Arabian plates. Its spreading rate is also slow with a full rate of 20–30 mm/year. This suggests that the mantle contains some amount of water and is dehydrated by partial melting beneath the ridge independent of the spreading rate and the spreading regime (normal oceanic spreading or back-arc spreading). The mantle conductivity beneath the spreading ridges is controlled primarily by the presence of water rather than by the thermal structure.

Baba et al. (2004a) further discuss the partial melt zone in the MELT model shown in (Figure 3c). The relatively conductive area below 60 km in the vicinity of the SEPR axis of the anisotropic model is likely to result from the presence of at most 1% partial melt. The melt zone is quite broad; it is asymmetrically wider to the west. This asymmetry is consistent with results from previous study (Evans et al., 1999) and seismic studies (e.g., Toomey et al., 1998; Dunn and Forsyth, 2003). A narrow, highly conductive zone in the vertical direction is merely suggested by the data, not strongly indicated. The difference in melt fraction among the coordinate directions probably corresponds to the difference in connectivity of the melt. The narrow conductive zone suggests that the melt is more highly connected in the vertical direction beneath the rise axis.

Heinson et al. (2000) discussed melt transport mechanisms from the mantle to the magma chamber in the crust. They inverted the MT responses observed in the Reykjanes Ridge as a part of the Reykjanes Axial Melt Experiment: Structural Synthesis from Electromagnetics and Seismics (RAMESSES) experiment (Sinha et al., 1998). The obtained 1D models show high conductivities in the upper 10 km, which are consistent with the crustal conductivities derived from CSEM measurements (MacGregor et al., 1998), a resistive zone in ~10–50 km depth with resistivity values above 100 Ωm, and again high conductivities at 50–70 km depth. Heinson et al. (2000) compared the results with the 1D conductivity model obtained at the Axial Seamount, Juan de Fuca Ridge (Heinson et al., 1996; Constable et al., 1997), which shows high conductivity (~10 Ωm) even above 60 km depth, and argued that the upper few tens of kilometers of the mantle beneath the Reykjanes Ridge were periodically drained of magma. It is extracted upwards rapidly to create large but ephemeral crustal magma chambers.

3.2. Crustal accretion processes

The melt migrates from its source region in the deeper mantle to a narrow zone centered beneath the ridge axis, where it forms an axial magma chamber (AMC) in the depth range of ~1.5–7 km beneath the seafloor. Differentiated magma in the AMC intrudes into the shallow crust and erupts at the seafloor. These zones are recognized as layers 2B/C and 2A, respectively, in terms of seismic P-wave velocity, or as sheeted dikes and pillow basalts in ophiolites. Crystallized magma in the AMC is inferred to form layered gabbros (layer 3).

Recent marine EM studies have revealed the AMCs for both fast and slow spreading ridges. MacGregor et al. (1998) analyzed CSEM data collected within the RAMESSES experiment and obtained a 2D conductivity model of the crust beneath the Reykjanes Ridge at 57°45′N using a forward modeling approach. The obtained model shows a conductive (2.5 Ωm) trapezoidal zone at ~2 km depth beneath the ridge crest. It is attributable to the presence of basaltic melt with a fraction of at least 20%. That zone is coincident with the low velocity zone required by seismic data; it is interpreted as the AMC.

Key and Constable (2002) present a 2D conductivity model of the crust and shallow mantle beneath the East Pacific Rise (EPR) at 9°50′N. The MT survey was conducted using four broadband marine MT instruments (Constable et al., 1998). The extended high-frequency performance of the instrument allows resolution of the electrical resistivity structure at shallower depths than those that are accessible using traditional marine MT sensors. The obtained 2D inversion model shows a conductive zone in the middle crust that extends about 3 km on both sides of the ridge axis at depths of ca. 1.5–6 km below the seafloor and has resistivities of about 1–100 Ωm, indicating the AMC (Figure 4). It coincides with a low P-wave velocity zone detected at 9°30′N using seismic tomography and a low shear velocity region detected at 9°48′N using seafloor compliance results. The estimated melt fraction in the high-conductivity zone is about 1–20%, which is in agreement with the seismic results. A total melt volume of about 0.75 km^3 per kilometer of ridge implies an average melt residence time of about 1000 years.

3.3. Shallow crustal structure and hydrothermal circulations

In the uppermost crust at the ridge, porosity and hydrothermal circulation control the conductivity structure. The amount of seawater within the crust, its distribution, and its temperature and salinity are all parameters that influence electrical conductivity.

Two MMR experiments are reported respectively by Evans et al. (1998, 2002). The former experiment was carried out using three seafloor instruments and 34 transmission stations in the Cleft–Vance overlapping spreading center of the Juan de Fuca (JDF) ridge. The latter experiment took place

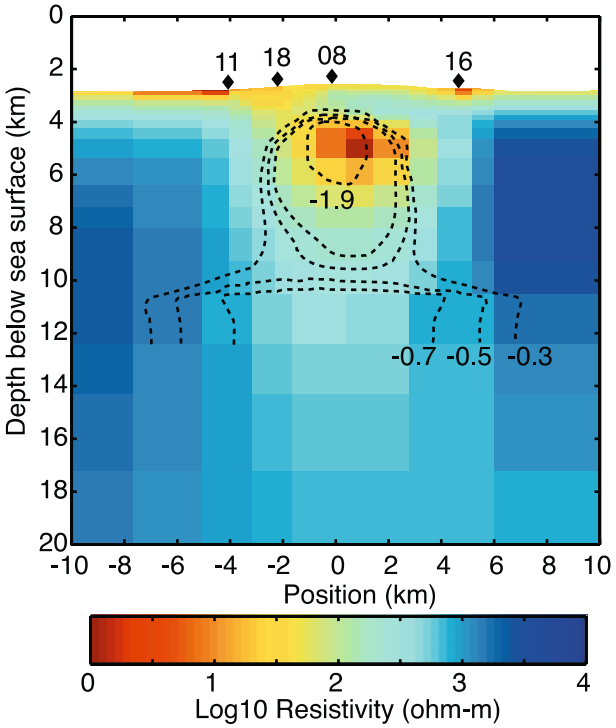

Figure 4. 2D resistivity model of the crust and uppermost mantle beneath the EPR at 9°50′N (Key and Constable, 2002). Diamonds indicate site locations. Superimposed contour lines are seismic velocity perturbation in units of km/s from Dunn et al. (2000).

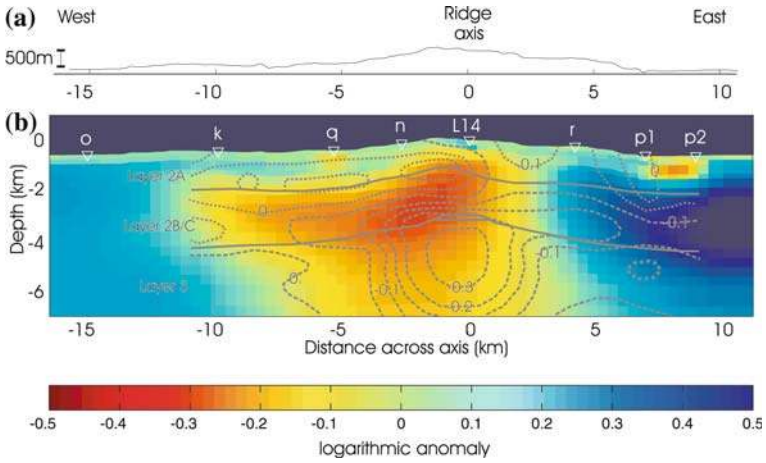

Figure 5. 2D crustal resistivity structure beneath the VFR (MacGregor et al., 2001): (a) the bathymetry; (b) the resistivity anomaly calculated relative to an average 1D resistivity structure. Labeled triangles indicate the position of receivers. Superimposed dotted lines are the seismic velocity anomaly in units of km/s calculated by Turner et al. (1999).

together with the broadband MT survey in the EPR at 9°50′N reported by Key and Constable (2002). Ten instruments were deployed and more than 200 transmission stations were completed during the experiment. In both the areas, the conductivity of the uppermost crust (less than 1 km depth) is more resistive for off-axis (about 10 Ωm) than at the axial zone (0.3–0.4 Ωm at the JDF and ~5 Ωm at the EPR). Evans et al. (2002) explain that the uppermost few hundred meters of crust are much hotter beneath the ridge crest than the off-axis, lowering the pore-fluid conductivity. Despite the fact that the EPR at 9°50′N is a much more hydrothermally active area than the Cleft segment, they further argue that hot fluids flow in spatially limited fissures on the EPR and have less impact on the bulk resistivity. In contrast, at the Cleft, the seafloor is more extensively faulted, thereby distributing hot fluids over a larger area of the seafloor.

MacGregor et al. (2001) report on a CSEM study on the Valu Fa Ridge (VFR) at 22°25′S in the Lau Basin. The VFR is a back-arc spreading center with intermediate spreading rate (60–70 mm/year) and a site of extensive hydrothermal activity. The CSEM experiment was part of a multidisciplinary study which included reflection and refraction seismics, bathymetry and potential field measurements. EM signals at frequencies between 0.25 and 40 Hz were transmitted from a horizontal electric dipole towed close to the seafloor. Data were recorded using an array of 11 receivers at distances of up to 20 km from the source. Data were interpreted using a combination of 1D and 2D forward modeling and inversion. The 2D inversion model is characterized by abnormally low resistivities (< 10 Ωm) with a small vertical gradient in layer 2B/C above the magma chamber, in a region where the seismic velocity anomaly is small (Figure 5). This chamber is much more conductive than the crust at equivalent depth beneath the axis of the slow-spreading Reykjanes Ridge at 57°45′N (MacGregor et al., 1998), and the fast-spreading EPR at 13°N (Evans et al., 1994). The lack of a vertical conductivity gradient in layer 2 also contrasts with the results of the seismic velocity structure, suggesting that the electromagnetic and seismic data are sensitive to very different physical properties of the crust. The high conductivity coupled with the low seismic velocity anomaly in layer 2B/C at the axis can be explained by the pervasive penetration of hot and saline fluids produced by phase separation in the axial hydrothermal system or released from the melt body.

MacGregor et al. (2002) further studied the properties of crustal fluids at the VFR and their relationship to active hydrothermal circulation from joint analysis of electromagnetic and seismic data presented by Greer et al. (2002). At a distance of 4.2 km east of the axis, the electric and elastic properties can be explained by the two-phase medium consisting of seawater at ambient ocean floor temperatures (3 °C) permeating a solid rock matrix. The fluid fraction of approximately 4% and a crack aspect ratio of about 0.017 give the

best fit to the data. However, at the ridge axis, the assumption of two-phase medium no longer holds.

4. Mantle Upwelling and Downwelling Regions

4.1. Mid-mantle structure

The mid-mantle conductivity structures beneath the Pacific and the Philippine Sea plates are presented by Koyama (2002), Utada et al. (2003), and Fukao et al. (2004). Those studies were intended to portray the heterogeneity of the mid-mantle beneath Hawaii and the west Pacific subduction zone – both regions of typical mantle upwelling and downwelling. The data set used in the studies comprises the electric field variation obtained by submarine cables crossing the Philippine Sea and Pacific Ocean and magnetic field variations obtained by circum-Pacific observatories and long-term observation sites. The MT and GDS responses were calculated for eight discrete periods at each observation station and cable location respectively during 1–8 days for the MT data and 5–27 days for the GDS data. The responses were corrected for the effect of 3D land–ocean distribution and inverted iteratively; then 1D models explaining all the relevant data were obtained. The preferred model is a smooth conductivity-depth profile with two abrupt jumps that possibly correspond to the seismic discontinuities at 410 and 660 km depth. The model agrees well with the 1D profile inferred from the laboratory study by Xu et al. (1998). The 1D model can be used as a reference electrical conductivity model of the Earth's mantle beneath the North Pacific region (Utada et al., 2003).

The responses were further inverted to a 3D model of conductivity perturbation from the 1D reference conductivity. The resultant model shows a highly conductive transition zone beneath Hawaii and a transition region beneath the Philippine Sea that is conductive at depths above 550 km and resistive below. Fukao et al. (2004) compared the 3D conductivity anomaly model with results of global seismic tomography studies. The P-wave velocity anomalies and the electrical conductivity anomalies were converted respectively to temperature anomalies using a proposed conversion formula and experimental results for mantle minerals. Figure 6 shows cross-sections of the models across Hawaii and the Philippines. Resultant temperature anomalies show consistently positive temperature anomalies of 200–300 K in the mantle transition zone beneath the Hawaiian hotspot. At the subduction zones, where slab-related negative anomalies and mantle wedge related positive anomalies are likely to coexist in close proximity, seismic and EM tomography do not always give consistent results. Negative temperature anomalies of 200–300 K associated with the slab stagnant in the transition zone beneath the Philippine Sea are resolved clearly in the seismic tomography, but are not

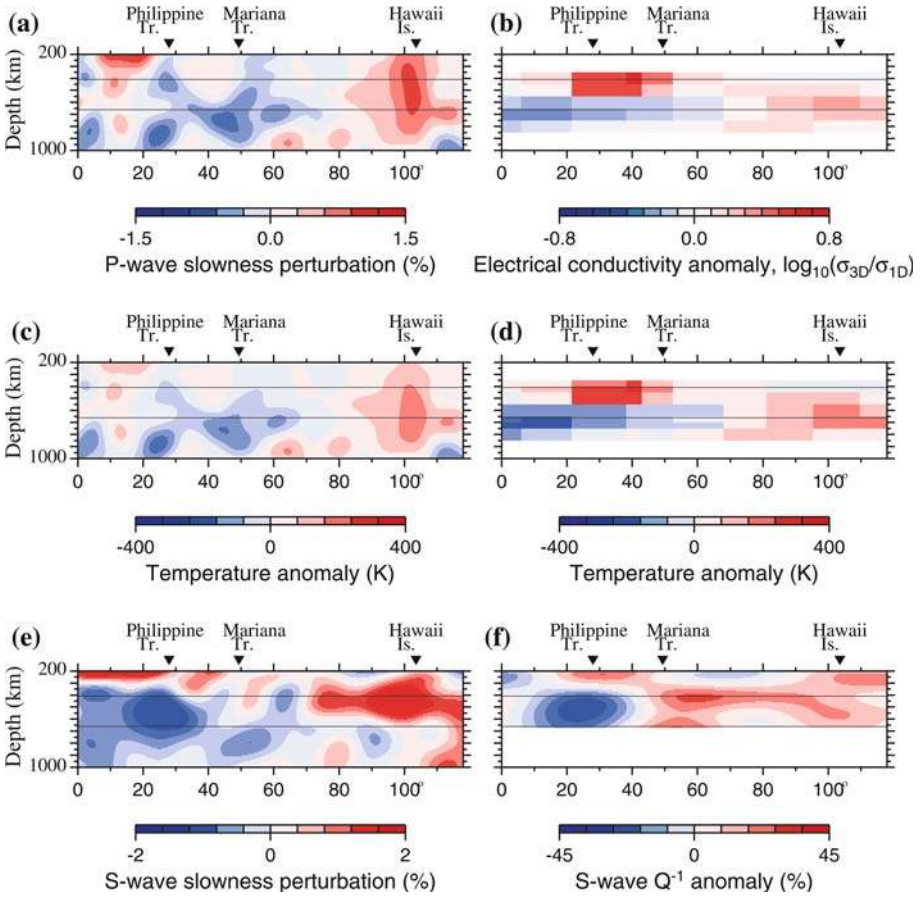

Figure 6. Cross-sections of the seismic and EM tomography results along a profile across Hawaii and Philippine (Fukao et al., 2004): (a) P-wave velocity anomalies; (b) electrical conductivity anomalies; (c) temperature anomalies converted from P-wave velocity anomalies; (d) temperature anomalies converted from electrical conductivity anomalies; (e) S-wave velocity anomalies; (f) S-wave Q^{-1} anomalies.

visible through the use of EM tomography. On the other hand, the positive-temperature anomaly in the intervening zone between the Mariana slab and the Philippine slab is pronounced in the EM tomography, but marginal in the seismic tomography.

4.2. Upper mantle structure in hotspot regions

The origin of upwelling plumes is thought to be deep, at least in the mantle transition zone or possibly the core-mantle boundary. The intensity of the thermal anomaly, its extent and the melting processes producing oceanic

island basalt (OIB) can be investigated using marine EM methods. At least two marine EM studies have examined mantle upwelling regions.

Nolasco et al. (1998) describe an MT experiment using six instruments around the Society Islands hotspot. The 2D inversion of the data set yields a model with slightly enhanced conductivities down to 130 km depth beneath the active hotspot area relative to a reference site located about 150 km distant from the active area. The mantle below 130 km is resistive compared to the surrounding area. Nolasco et al. (1998) argue that the central structure of the model differs greatly from the mean mantle model and can be associated with the hotspot plume. The higher conductivity can be explained by a small amount of melt (1–2.4%). Below 130 km, the high resistivities are apparently contradictory with the presence of rising hot material, but depletion of melt and volatiles could be a possible explanation.

The conductivity structure beneath the Hawaiian hotspot has been studied by Constable and Heinson (2004). Seafloor MT data were collected at seven sites across the Hawaiian hotspot swell, extending between 120 and 800 km southwest of the Hawaiian-Emperor Island chain. 2D smooth inversion of the data revealed a model with two major features: a resistive lithosphere underlain by a conductive mantle and a narrow plume-like conductive structure connecting the surface of the islands to the lower mantle (Figure 7). Forward modeling indicates that the data require the plume, but its location is outside of the observation area. The radius of the plume appears to be less than 100 km. The resistivity of around 10 Ωm extending to a depth of 150 km is consistent with a bulk melt fraction of 5–10%. An observed seismic low-velocity zone at depths centered around 60 km and extending 300 km from the islands is not reflected in the conductivity model where high lithospheric resistivities extend the edge of the conductive plume. Constable and Heinson (2004) report that further forward modeling results suggest a hot and dry lithosphere model of thermal rejuvenation, or possibly underplated lithosphere depleted in volatiles resulting from melt extraction.

4.3. Upper mantle and crustal structure in the subduction zone and marginal basins

Mantle downwelling regions, where the oceanic lithosphere is subducted into the deep mantle, are characterized by trenches, volcanic arcs, and, in some regions, back arc basins. Water plays an important role in these areas because the subducting slab delivers water into the back arc mantle. It subsequently contributes to volcanic activity and back-arc dynamics.

The Philippine Sea plate is the biggest marginal basin. It is thought to have been formed by successive back-arc opening of the West Philippine Basin (WPB), the Shikoku-Parece Vela Basin (PVB), and the Mariana Trough, associated with the westward subduction of the Pacific plate. The

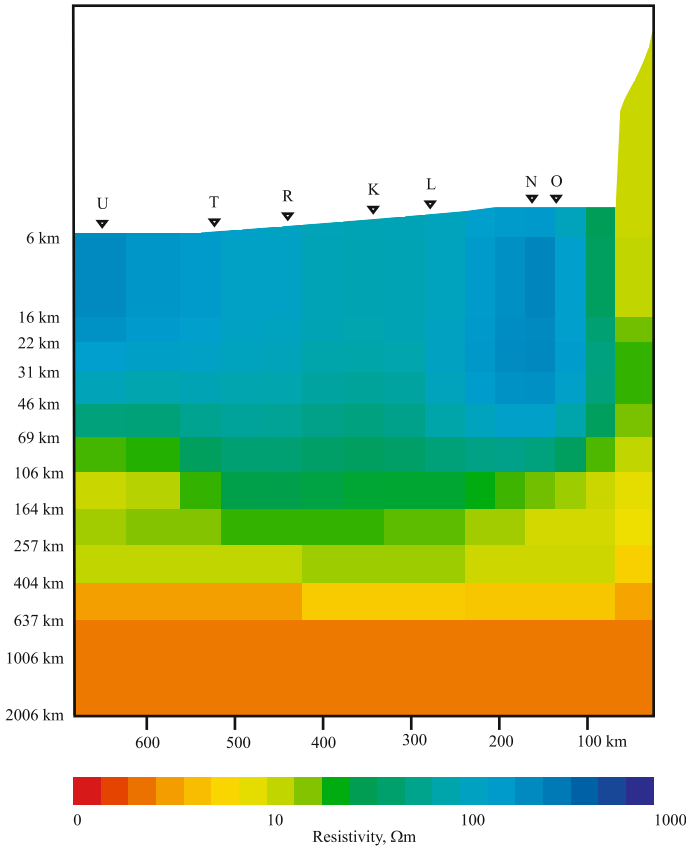

Figure 7. 2D mantle resistivity model beneath the Hawaiian hotspot swell region (Constable and Heinson, 2004). Triangles indicate site locations projected to the NE-SW profile.

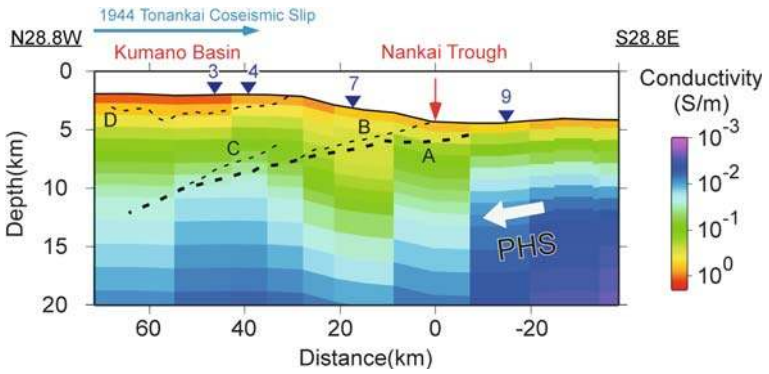

Figure 8. 2D crustal conductivity model beneath the Nankai Trough (Goto et al., 2003). Triangles indicate the site locations used for analysis. Seismic reflectors by Park et al. (2002) are shown as broken lines. 'PHS' denotes the Philippine Sea plate.

Philippine Sea plate involves various tectonic settings and is therefore an excellent field laboratory for geophysical studies. The Mariana Trough is now an active back arc basin. It is regarded as a desirable area for the study of the dynamics associated with plate subduction and back-arc opening. The northwest edge of the Philippine Sea plate is subducting beneath the Eurasian plate at the Nankai Trough and the Okinawa Trough, which are both characterized with high seismicity. A salient feature of the Philippine Sea is the linear relationship between the water depth and the square root of the crustal age, but excess depth of ~800 m compared with the depth of other major ocean of the same age (Park et al., 1990).

A marine MT and seismic experiment took place across the Philippine sea in NW-SE direction during 1999–2000. For MT measurements, six instruments were deployed in the WPB, PVB, and the Mariana Trough. Seama et al. (2004) analyzed the data and obtained 1D conductivity models at four sites at seafloor locations of different crustal ages. The models are well related to the crustal age of each site, except for the site near the axis of the Mariana Trough. The relation between the water depth and the crustal age is indistinguishable from that observed in the North Pacific (Heinson and Constable, 1992). However, the seismic study demonstrates that the Rayleigh wave phase velocity is also related to the crustal age, but is remarkably lower than that observed in the region of the same age in the Pacific (Isse et al., 2004). These observations suggest that the anomaly of the Philippine Sea is not attributable to a thermal anomaly in the upper mantle. Seama et al. (2004) speculated that the depth anomaly may be caused by dynamic topography. Isse et al. (2004) argue that the depth anomaly and the seismic results may be explained by iron-abundance in the mantle.

A marine MT survey across the Mariana Trough at 18°N is reported in Goto et al. (2002). Ten instruments were deployed in 2001–2002 along a transect covering the Pacific plate, the Mariana Trough, and the PVB. Baba et al. (2004b) analyzed data that were recovered from five sites and data from three sites collected in previous experiments (Filloux, 1983; Seama et al., 2004). The 2D conductivity models of the upper mantle they obtained, show an increase in conductivity at the depth of 70 km beneath the Mariana Trough. Below 70 km, the model derived from TM mode inversion is slightly more conductive than the model obtained from TE mode inversion, which might indicate an anisotropy that is more conductive perpendicular to the strike even though the anisotropy is not strongly dictated by the data. The mantle beneath the Mariana Trough and the PVB seems somewhat more conductive than the mantle beneath the Pacific plate, suggesting a hot thermal anomaly and an abundance of water in the back-arc mantle.

Goto et al. (2003) describe a marine MT experiment using nine broadband instruments and two standard instruments in the Nankai Trough South of Japan. The study area is characterized by the northwest subduction of the

Philippine Sea plate beneath the Eurasian plate including Japan. It has a pronounced seismogenic zone with the repeated occurrence of magnitude-8 class mega-earthquakes. Data from four broadband instruments were analyzed and used to derive the 2D conductivity model shown in Figure 8. The model shows a conductive upper crust of the Philippine Sea plate ($\sim$10 Ωm) below the axis of the Nankai Trough. The conductivity decrease below $\sim$10 km depth, $\sim$30 km towards the Kumano Basin, which coincides approximately with the front edge of the rupture zone of the 1944 Tonankai earthquake. This coincidence suggests that the release of fluid from the crust of the Philippine Sea plate occurs within the subduction process and results in locking between the overlying and subducting crusts, which would cause earthquakes.

5. Discussion

The electrical conductivity of oceanic lithosphere and asthenosphere and their age dependency was among the first targets of marine MT studies. It was actively studied until the early 1990s (e.g., Oldenburg, 1981; Heinson and Constable, 1992), but has only been rarely addressed since then. Therefore, except for mention of the study of Philippine Sea plate (Seama et al., 2004), it was not explicitly discussed in the previous sections. However, recent studies of MELT data have revealed an age-independent conductivity pattern for the young ($< \sim$3 Myear) lithosphere and asthenosphere, which can be explained by water distribution rather than thermal structure (Baba et al., 2004a; Evans et al., 2005). For that reason, discussion is included herein of the apparent inconsistency in conductivities for the young and the matured lithosphere and asthenosphere. This section presents a new laboratory-based conductivity model and examines whether or not the laboratory-based model can explain the MT-based models for a mature lithosphere and asthenosphere.

Heinson and Constable (1992) presented a laboratory-based conductivity model to explain the MT models. It takes into account the thermal structure due to lithospheric cooling and partial melt. Their laboratory-based model is, however, systematically more resistive than the MT-based models even though it reproduced the age-dependent pattern. The inconsistency was attributed to the coast effect although the impact of the coast effect has remained controversial (Tarits et al., 1993; Constable and Heinson, 1993). Since Karato (1990) proposed that water enhances the conductivity markedly, the high-conductivity zone has been interpreted preferably as the effect of water (e.g., Lizarralde et al., 1995). Moreover, their laboratory-based model cannot explain the age-independent resistive–conductive transition at $\sim$60 km depth for young mantle.

Hereafter, the laboratory-based model is revised, superimposing the effect of water redistribution caused by partial melting at mid-ocean ridges on the thermal structure. A thermal structure is first calculated based on the plate-ecooling model (Turcotte and Schubert, 2002), which well explains observed bathymetric change with age. The potential temperature and plate thickness are assumed to be 1350 °C and 125 km is assumed as the respectively. An adiabatic temperature gradient of 0.3 °C/km is added. This thermal structure model is almost identical to the model used by Heinson and Constable (1992). The obtained thermal structure is plotted as profiles to the depth every 10 Myear in Figure 9 and as isotherm on the depth–age plane in Figure 10a.

The conductivity model is estimated based on Ichiki et al. (2004b), who present calculation of Hashin–Shtrikman (HS) bounds for multi-phase systems (Park and Ducea, 2003) based on pyrolitic mineral assemblage. The calculations take into account the enhancement of the conductivity caused by dissolved hydrogen (Karato, 1990), not only in olivine, but also in orthopyroxene (opx), clinopyroxene (cpx), and garnet. The mantle composition is assumed according to Hirth and Kohlstedt (1996): it consists of 56% olivine, 19% opx, 10% cpx, 15% garnet (i.e., garnet pyrolite), and 810 ppm H/Si water in olivine and an appropriate amount of water in opx, cpx, and garnet calculated using the partition coefficients. A transition exists among garnet, olivine, and pyroxene at 40–70 km depth. Consequently, the composition of 55% olivine, 27% opx, and 18% cpx above the transition depth is assumed

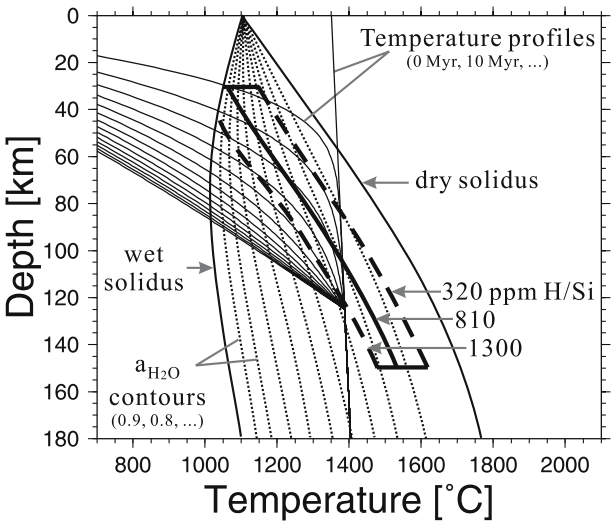

Figure 9. Temperature–pressure phase diagram from Hirth and Kohlstedt (1996). The bold solid line and dashed lines represent solidi for mantle assemblages containing water of 810 ± 490 ppm H/Si in olivine. Temperature profiles based on the plate-cooling model are superimposed.

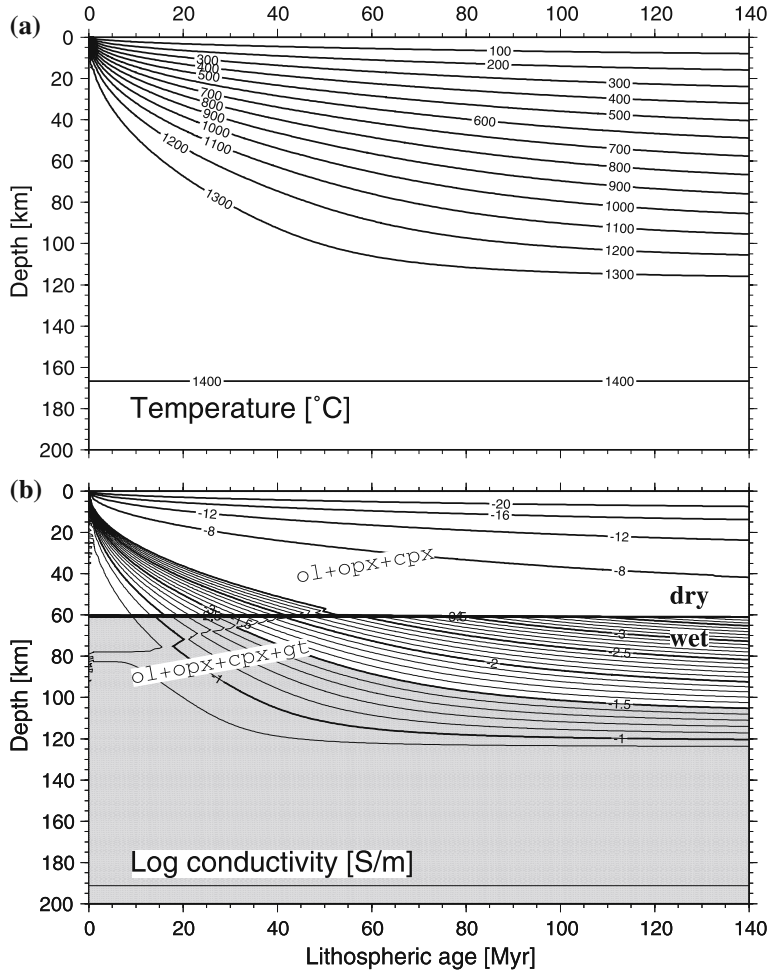

Figure 10. (a) Thermal structure model based on the plate-cooling model. (b) HS upper bound for the conductivity of a pyrolite mantle. Annotations of the contour lines show log conductivity. Note the change in the contour interval at 10^{-4} S/m for clarity. The region that is more conductive than $10^{-1.5}$ S/m is shaded gray.

according to Park and Ducea (2003). The transition depth is calculated from the phase diagram of Green and Ringwood (1970). The experimental data for the conductivity of each mineral and diffusion of hydrogen, which were compiled by Ichiki et al. (2004b), are used to calculate the bulk conductivity, except for the olivine data. Here, the applied dry olivine conductivity data are those measured by Constable et al. (1992); the diffusivity data for hydrogen in olivine are those measured by Kohlstedt and Mackwell (1998).

Figure 9 shows a temperature–pressure phase diagram from Hirth and Kohlstedt (1996) together with the temperature profiles calculated in this

study. Beneath the mid-ocean ridge (i.e., 0 Myear) the temperature profile intersects the dry solidus at about 60 km depth. Consequently, the dry–wet boundary is assumed to be located at 60 km depth. The enhancement of conductivity caused by partial melt is ignored because the matured mantle is discussed here. The temperature profiles for the age younger than 30 Myear intersect the wet solidus containing water of 810 ppm H/Si, but never intersect the dry solidus. Because the melt fraction and resulting hydrogen extraction from solid phases are very limited in the depth between wet and dry solidi (Hirth and Kohlstedt, 1996; Karato and Jung, 1998) and solid phases containing hydrogen are highly conductive, such a small amount of melt below 60 km does not greatly affect the bulk conductivity.

The anisotropic conductivity associated with the lattice preferred orientation (LPO) of minerals should be considered because it is likely to occur at asthenospheric depth, as the MELT data indicated. The LPO patterns of olivine, opx, and cpx are summarized in Mainprice et al.(2000). According to Mainprice et al. (2000), olivine [100] axis and opx [001] axis are subparallel to the shear direction (= plate spreading direction). The knowledge of cpx fabrics is rather poor, but the [001] axis seems to be close to the shear direction. Hydrogen diffusivity data are available for all axes of olivine (Kohlstedt and Mackwell, 1998), only the [001] axis of opx (Woods and Mackwell, 1999), and the [100] and [001] axes of cpx Woods et al., 2000). Garnet is isometric and its data are provided by Wang et al. (1996). The fastest axes are [100] for olivine, [001] for opx, and [100] (but comparable to [001]) for cpx, respectively, corresponding to the axes that are subparallel to the shear stress direction. Consequently, the HS upper bound is calculated for the assemblage of olivine [100], opx [001], cpx [001], and garnet, which gives the upper limit of possible conductivity.

Figure 10b is the resultant conductivity distribution as a function of depth and lithospheric age. The iso-conductivity lines are primarily parallel to the isotherms (Figure 10a). For younger age, the conductivity jumps slightly at the phase transition depth (60–80 km) because of the relatively low conductivity of garnet. The dry–wet transition at 60 km enhances the conductivity greatly for the entire range of age. However, defining the zone with conductivity higher than $10^{-1.5}$ S/m as the conductive zone (gray shaded zone in Figure 10b), the resistive–conductive transition is sharp and its depth is unchanged at 60 km for ages younger than about 30 Myear, but the transition is gradual and its depth increases with depth for older age. This gradual transition exists because the hydrogen contribution to the conductivity is proportional to the hydrogen diffusivity (Karato, 1990), which is also a function of temperature, decreasing exponentially concomitant with decreasing temperature (e.g., Kohlstedt and Mackwell, 1998). The conductivity structure again ceases to change with age for mantle older than $\sim$100 Myear, reflecting the slight temperature variation.

The lower limit of possible conductivity is also assessed. The HS bounds of the conductivity are calculated for the combination of olivine [001], opx [001], cpx [010], and garnet. Although the alignments of such axes are unlikely, it is useful to see the lower limit of the possible conductivity. The [001] axis of opx is used for both alignment patterns because of the lack of data for the other axes. The hydrogen diffusivity for the [010] axis of cpx is not well constrained, but it seems to be about one order smaller than the other directions (Woods et al., 2000); thereby, the value of a tenth of the diffusivity in the [001] axis is assumed for the [010] axis. Figure 11 shows conductivity profiles for 20 Myear age mantle. Solid lines demarcate the HS upper and lower bounds for the alignments of the fastest diffusion axes. The HS upper bound corresponds to the conductivity shown in Figure10b. Dashed lines delimit the HS bounds for the alignment of the slowest diffusion axes. The difference between the upper bounds of the former alignment pattern and the lower bound of the latter pattern indicates that the maximum anisotropy attributable to the crystallographic alignments is, at most, a factor of 10.

The laboratory-based conductivity model is compared with 1D inversion models for the mantle of variable ages obtained by Heinson and Constable (1992), Heinson and Lilley (1993), Nolasco et al. (1998), Seama et al. (2004), Ichiki et al. (2004a)(Figure 12). Note that the conductivity profiles from the laboratory-based model plotted in the figure are the upper bounds for alignments of the fastest axes so that the lower limits are about one order smaller than the values shown by the lines. However, the profiles are obtained

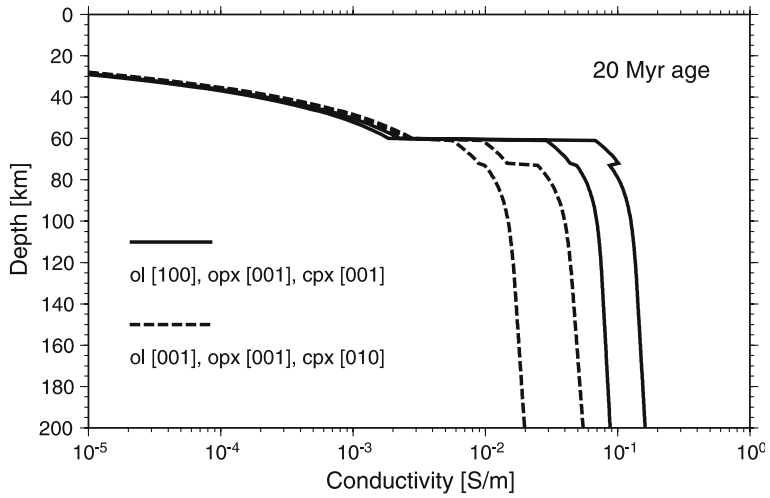

Figure 11. HS upper and lower bounds of the laboratory-based conductivity model for 20 Myear age mantle. Solid lines show the bounds in the case that the minerals align their LPOs. Dashed lines are the bounds in the case that the axes of slowest hydrogen diffusion are selected.

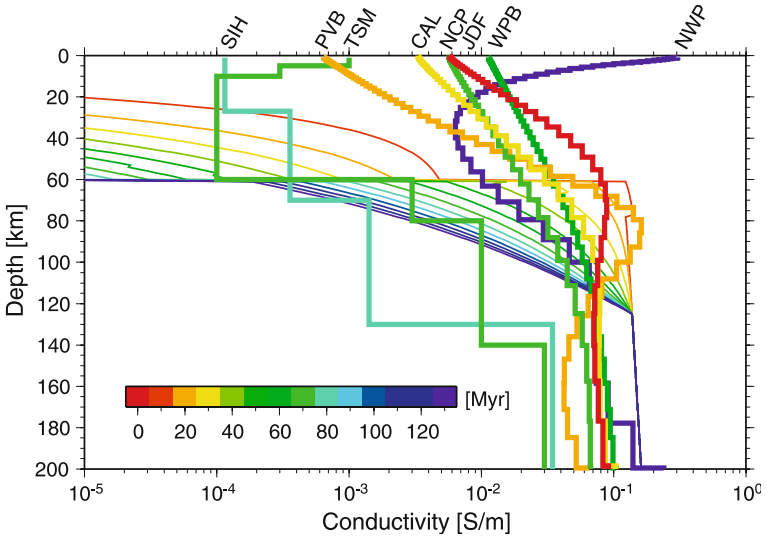

Figure 12. Conductivity profiles for every 10 Myear from the laboratory-based model (thin lines) and inversion models obtained by various researchers (thick lines). The laboratory-based profiles are the upper limit of the possible conductivity, as discussed in the text. GRAY SCALE indicates the lithospheric age. The inversion models – JDF (near Juan de Fuca ridge: 1 Myear), CAL (off California: 30 Myear), NCP (North Central Pacific: 72 Myear) – are from Heinson and Constable (1992); NWP (North West Pacific: ~130 Myear) is from Ichiki et al., (2004b), PVB (Parece-Vela Basin: 21 Myear) and WPB (West Philippine Basin: ~60 Myear) are from Seama et al. (2004); SIH (Society Island Hotspot: ~70 Myear) is from Nolasco et al. (1998); and TSM (Tasman Sea: ~60 Myear) is from Heinson and Lilley (1993).

from the observations by assuming an isotropic conductivity structure. Inversion models for the North Pacific (JDF, CAL, NCP, and NWP) and the Philippine Sea (PVB and WPB) resemble one another and the laboratory-based model, whereas the models for the Tasman Sea (TSM) and Society Island hotspot (SIH) are more resistive than the others.

Conductivities of the first group converge to around 0.08 S/m below ~130 km depth independent of the lithospheric age. The changes in conductivity with depth are small compared with those above ~130 km depth. These profiles agree well with the laboratory-based conductivity models in the depth range where changes in conductivity are controlled only by the adiabatic temperature gradient. The inversion models are slightly more resistive than the laboratory-based model, which does not conflict with the possible limit of the laboratory-based conductivity shown in Figure 11. Between the depths of 60 and ~130 km, a clear age dependency is apparent, except for PVB. For both the inversion and laboratory-based model, the conductivity for older mantle decreases more at shallower depths, but this trend is mild for the inversion models. The abrupt change in conductivity

around 60 km depth never appears in the inversion models because these models were obtained by Occam inversion (Constable et al., 1987), which constrains the model to be smooth. Above 60 km depth, the laboratory-based model shows very low conductivity because of the dry condition and low temperature. However, the inversion models do not show such features, probably because the MT method is less sensitive to such a resistive zone. The resistive uppermost mantle and the abrupt increase in the conductivity at 60 km may be obtained if the data are inverted along with relaxation of the smoothness constraint at the depth as Utada et al. (2003) did for the study of mid-mantle structure.

The TSM model below 60 km depth is more resistive than the laboratory-based model, but the trend is similar. The mantle beneath the Tasman Sea may have similar thermal structure, but it contains less water than the mantle in the North Pacific and in the Philippine Sea. The large increase in conductivity at 60 km is obtained by forward modeling, giving the boundary depth a priori (Heinson and Lilley, 1993). Consequently, the depth is not constrained objectively. The fact that such a model was preferred by the authors is not opposed to the concept underlying the laboratory-based model. The SIH model is also resistive below 60 km, but an abrupt change in conductivity appears at 130 km depth. This change is not explained by the laboratory-based model; it seems to be something special. Although the SIH model plotted in Figure 12 is the structure beneath a site locating away from the hotspot swell region, the effect of the plume may reach the site.

6. Conclusions and remarks

During the last decade, marine EM studies have increasingly progressed by virtue of support from technical advancement, data accumulation, and interpretation based on multidisciplinary approaches.

Developments of new instruments have extended the exploration range toward both shallower and deeper structures. Modeling and inversion techniques have improved to address typical problems for marine EM studies, such as topographic and ocean/continent contrast effects, controlled-source methods, anisotropy, etc. Furthermore, 2D analysis became a standard approach. Challenges to those studies for 3D and anisotropic structures will become continue to increase in popularity in the next decade. Such studies will require additional efforts toward increasing data quality and density and improvement of analytical methods.

For studies of mid-ocean ridges, highly conductive zones have been identified with hydrothermal circulation and AMC in the crust and partial melt zones of MORB source in the mantle. Studies of hydrothermal circulation have typically used 1D and 2D inversions. However, these hydro-

thermal systems change spatially and even temporally. Thus, 3D and 4D analyses that include time variations can pose challenging themes to guide future studies. Many seafloor MT experiments have been conducted in the EPR and have contributed towards the understanding of the melt generation and crust accretion processes that occur beneath fast-spreading ridges. However, the connection between the source region and the AMC remains unclear. The connection is expected to be elucidated by a recent experiment of the Scripps group, in which both broadband MT and CSEM were jointly conducted in 2004 at 9°30–50′N in the EPR (Key and Constable, 2004). Detailed imaging of the partial melt zones in the AMC and the deeper mantle beneath slow spreading ridges is also interesting for future studies. Those areas are also good fields for 3D studies because plume-like upwellings beneath the ridge axis are expected in slowly spreading ridges.

Several studies have been reported in both mantle upwelling and downwelling regions. Conductivity structures in the mid-mantle beneath the Hawaii hotspot region and the Philippine Sea plate show anomalies that are consistent with seismic velocity anomalies in terms of the temperature perturbations. The upper mantle conductivity beneath the hotspots in Hawaii and in the Society Islands somewhat contradict the idea that the zone inferred as a plume is either more conductive or more resistive than the surrounding mantle. Further case studies in various hotspot regions are necessary to find general features of the upwelling plumes. The conductivity structures of subduction zones surrounding the Philippine Sea plate have been studied. The conductivity models obtained are suggestive of dehydration of the subducting slab. Further studies with high-resolution modeling are expected to confirm the dehydration phenomenon. A dense MT survey in the Mariana subduction system has been planned for 2005–2006. It is a large, international collaborative study that is organized similarly to the MELT experiment (N. Seama, pers. commun., 2004).

Conductive zones coincide with seismic low-velocity zones in most tectonic settings. Some exceptions suggest a different response of electrical conductivity and seismic velocity to the parameters that determine the tectonic structure. Comparison of the conductivity models with seismic velocity models, laboratory experiments, and other observations, is necessary to understand and separate the effects of the parameters. Therefore, such comparisons have become common, and quantitative parameter separation has been attempted in some studies. This approach is likely to be undertaken more commonly in future studies as multidisciplinary experiments increase.

Water has been recognized as playing a key role in mantle dynamics. Redistribution of water caused by the partial melting process at mid-ocean ridges has been emphasized for the conductivity pattern of the oceanic lithosphere and asthenosphere. A new laboratory-based conductivity model for the mature oceanic lithosphere and asthenosphere is proposed. It takes into

account the water distribution in addition to the thermal structure. It well explains the conductivity model based on MT observations in the depth range of 60–200 km.

Acknowledgements

I would like to thank Prof. Baldev R. Arora and the Organizing Committee of the 17th Workshop on Electromagnetic Induction in the Earth in Hyderabad, India for the invitation to present this review. Many colleagues promptly provided reprints and pre-prints, but including all of them was beyond my capabilities. Masahiro Ichiki provided helpful comments on the construction of the laboratory-based conductivity model. Considerate advice by Katrin Schwalenberg and an anonymous reviewer improved the manuscript. The GMT software package (Wessel and Smith, 1998) was used to produce some of the figures.

References

Baba, K. and Chave, A.D.: 2005. 'Correction of Seafloor Magnetotelluric Data for Topographic Effects During Inversion', *J. Geophys. Res.*, in press.

Baba, K., Chave, A. D., Evans, R. L., Hirth, G., and Mackie, R.L.: 2004a. 'Mantle Dynamics Beneath the East Pacific Rise at 17°S: Insights from the MELT EM Data', *J. Geophys. Res.*, submitted.

Baba, K. and Seama, N.: 2002. 'A New Technique for the Incorporation of Seafloor Topography in Electromagnetic Modeling', *Geophys. J. Int.* **150**, 392–402.

Baba, K., Seama, N., Goto, T., Ichiki, M., Schwalenberg, K., Suyehiro, K. and Utada, H.: 2004b. 'Electrical Transection of the Upper Mantle in the Mariana Subduction System', in: *Proceedings of the 17th Workshop on Electromagnetic Induction in the Earth*, Hyderabad, India, October 18–23.

Chave, A.D. Constable, S.C. and Edwards, R.N.: 1991. *Electrical Exploration Methods for the Seafloor*, Vol. 2 of *Electromagnetic Methods in Applied Geophysics*, Chapt. 12, pp. 931–966, Soc. of Explor. Geophys., Tulsa, OK.

Chave, A.D. Evans, R.L., Hirth, J.G., Tarits, P., Mackie, R.L., Booker, J.R. and the MELT Team.: 2001. 'Anisotropic Electrical Structure Beneath the East Pacific Rise at 17°S', in: *OHP/ION Joint Symposium, Long-term Observations in the Oceans: Current Status and Perspectives for the Future*, pp. 119–123.

Chave, A. D. and Smith, J. T.: 1994. 'On Electric and Magnetic Galvanic Distortion Tensor Decompositions', *J. Geophys. Res.* **99**(B3), 4669–4682.

Constable, S. and Heinson, G.: 2004. 'Hawaiian Hot-spot Swell Structure from Seafloor MT Sounding', *Tectonophysics* **389**(1–2), 111–124, doi:10.1016/j.tecto.2004.07.060.

Constable, S. C. and Cox, C. S.: 1996. 'Marine Controlled-Source Electromagnetic Sounding. 2. The PEGASUS Experiment', *J. Geophys. Res.* **101**(B3), 5519–5530.

Constable, S. and Heinson, G.: 1993. 'In Defence of a Resistive Oceanic Upper Mantle: Reply to a Comment by Tarits, Chave and Schultz', *Geophys. J. Int.* **114**, 717–723.

Constable, S. C., Heinson, G. S., Anderson, G. and White, A.: 1997. 'Seafloor Electromagnetic Measurements above Axial Seamount, Juan De Fuca Ridge', *J. Geomag. Geoelectr.* **49**, 1327–1342.

Constable, S. C., Orange, A. S., Hoversten, G. M. and Morrison, H. F.: 1998. 'Marine Magnetotellurics for Petroleum Exploration. Part I: A Sea-Floor Equipment System', *Geophysics* **63**(3), 816–825.

Constable, S. C., Parker, R. L. and Constable, C. G.: 1987. 'Occam's Inversion: A Practical Algorithm for Generating Smooth Models from Electromagnetic Sounding Data', *Geophysics* **52**(3), 289–300.

Constable, S. C., Shankland, T. J. and Duba, A.: 1992. 'The Electrical Conductivity of an Isotropic Olivine Mantle', *J., Geophys. Res.* **97**(B3), 3397–3404.

De Groot-Hedlin, C. and Constable, S.: 1990. 'Occam's Inversion to Generate Smooth, Two-dimensional Models from Magnetotelluric Data', *Geophysics* **55**(12), 1613–1624.

Dunn, R.A. and Forsyth, D.W.: 2003. 'Imaging the Transition Between the Region of Mantle Melt Generation and the Crustal Magma Chamber Beneath the Southern East Pacific Rise with Short Period Love Waves', *J. Geophys. Res.*, **108**(B7): doi:10.1029/2002JB002217.

Dunn, R. A., Toomey, D. R. and Solomon, S. C.: 2000. 'Three-dimensional Seismic Structure and Physical Properties of the Crust and Shallow Mantle Beneath the East Pacific Rise at 9°30'N', *J. Geophys. Res.* **105**(B10), 23537–23555.

Evans, R.L., Hirth, G., Baba, K., Forsyth, D., Chave, A. and Mackie, R.: 2005. 'Compositional Controls on Oceanic Plates: Geophysical Evidence from the MELT Area', *Nature*, in press.

Evans, R. L., Sinha, M. C., Constable, S. C., and Unsworth, M. J.: 1994. 'On the Electrical Nature of the Axial Melt Zone at 13° N on the East Pacific Rise', *J. Geophys. Res.* **99**(B1), 577–588.

Evans, R. L., Tarits, P., Chave, A. D., White, A., Heinson, G., Filloux, J. H., Toh, H., Seama, N., Utada, H., Booker, J. R., and Unsworth, M. J.: 1999. 'Asymmetric Electrical Structure in the Mantle Beneath the East Pacific Rise at 17 °S', *Science* **286**, 752–756.

Evans, R. L., Webb, S. C., Jegen, M., and Sananikone, K.: 1998. 'Hydrothermal Circulation at the Cleft–Vance Overlapping Spreading Center: Results of a Magnetometric Resistivity Survey', *J. Geophys. Res.* **103**(B6), 12321–21338.

Evans, R.L., Webb, S.C. and the RIFT-UMC Team.: 2002. 'Crustal Resistivity Structure at 9°50'N on the East Pacific Rise: Results of an Electromagnetic Survey', *Geophys. Res. Lett.* **29**(6). doi:10.1029/2001GL014106.

Filloux, J. H.: 1983. 'Seafloor Magnetotelluric Soundings in the Mariana Island Arc Area Part II', in D. E. Hayes (ed.), *The Tectonic and Geologic Evolution of Southeast Asian Seas and Islands, Vol. 27 of Geophys. Monogr.*, AGU, Washington, DC, pp. 255–265.

Flosadóttir, A. H., Larsen, J. C., and Smith, J. T.: 1997. 'Motional Induction in North Atlantic Circulation Models', *J. Geophys. Res.* **102**(C5), 10353–10372.

Fujii, I., and Utada, H.: 2000. 'On Geoelectric Potential Variations over a Planetary Scale', *Memoirs of the Kakioka Magnetic Observatory* **29**, 1–81.

Fukao, Y., Koyama, T., Obayashi, M. and Utada, H.: 2004. 'Trans-Pacific Temperature Field in the Mantle Transition Region derived from Seismic and Electromagnetic Tomography', *Earth Planet. Sci. Lett.*, **217**, 425–434, doi:10.1016/S0012-821X0300610-1.

Goto, T., Kasaya, T., Mikada, H., Kinoshita, M., Suyehiro, K., Kimura, T., Ashida, Y., Watanabe, T., and Yamane, K.: 2003. 'Electromagnetic Survey of Fluid Distribution and Migration – An Example at the Nankai Seismogenic Zone', *BUTSURI-TANSA* **56**(6), 439–451(in Japanese).

Goto, T., Seama, N., Shiobara, H., Baba, K., Ichiki, M., Iwamoto, H., Matsuno, T., Mochizuki, K., Nogi, Y., Oki, S., Schwalenberg, K., Tada, N., Suyehiro, K., Mikada, H., Kanazawa, T., Fukao, Y., and Utada, H.: 2002. 'Geophysical Experiments in the Mariana Region: Report of the YK01-11 Cruise', *InterRidge News* **11**(1), 23–25.

Green, D. H., and Ringwood, A. E.: 1970. 'Mineralogy of Peridotitic Compositions Under Upper Mantle Conditions', *Phys. Earth Planet. Int.* **3**, 359–371.

Greer, A. A., Sinha, M. C., and MacGregor, L. M.: 2002. 'Joint Effective Medium Modelling for Co-incident Seismic and Electromagnetic Data, and its Application to Studies of Porosity Structure at Mid-Ocean Ridge Crests', *LITHOS Science Report* **4**, 103–120.

Groom, R. W., and Bailey, R. C.: 1989. 'Decomposition of Magnetotelluric Impedance Tensors in the Presence of Local Three-dimensional Galvanic Distortion', *J. Geophys. Res.* **94**(B2), 1913–1925.

Heinson, G.: 1999. 'Electromagnetic Studies of the Lithosphere and Asthenosphere', *Surv. Geophys.* **20**, 229–255.

Heinson, G., and Constable, S.: 1992. 'The Electrical Conductivity of the Oceanic Upper Mantle', *Geophys. J. Int.* **110**, 159–179.

Heinson, G., Constable, S., and White, A.: 1996. 'Seafloor Magnetotelluric Sounding above Axial Seamount', *Geophys. Res. Lett.* **23**(17), 2275–2278.

Heinson, G., Constable, S., and White, A.: 2000. 'Episodic Melt Transport at Mid-Ocean Ridges Inferred from Magnetotelluric Sounding', *Geophys. Res. Lett.* **27**(15), 2317–2320.

Heinson, G., and Lilley, F. E. M.: 1993. 'An Application of Thin-sheet Electromagnetic Modelling to the Tasman Sea', *Phys. Earth Planet. Int.* **81**, 231–251.

Hirth, G. and Kohlstedt, D. L.: 1996. 'Water in the Oceanic Upper Mantle: Implications for Rheology, Melt Extraction and the Evolution of the Lithosphere', *Earth Planet. Sci. Lett.* **144**, 93–108.

Ichiki, M., Baba, K., Araki, E., Hashimoto, Y., Suzuki, K. and Mizota, A.: 2004a. 'A Report on Kairei Cruise KR04-09', Technical Report, JAMSTEC (in Japanese).

Ichiki, M., Baba, K., Obayashi, M. and Utada, H.: 2004b. 'Water Content and Geotherm in the Upper Mantle above the Stagnant Slab: Interpretation of Electrical Conductivity and Seismic P-Wave Velocity Models', *Phys. Earth Planet. Int.*, submitted.

Isse, T., Shiobara, H., Fukao, Y., Mochizuki, K., Kanazawa, T., Sugioka, H., Kodaira, S., Hino, R., and Suetsugu, D.: 2004. 'Rayleigh Wave Phase Velocity Measurements Across the Philippine Sea from a Broad-band OBS Array', *Geophys. J. Int.* **158**, 257–266, doi:10.1111/j.1365-246X.2004.02322.x.

Karato, S.: 1990. 'The Role of Hydrogen in the Electrical Conductivity of the Upper Mantle', *Nature* **347**, 272–273.

Karato, S. and Jung, H.: 1998. 'Water, Partial Melting and the Origin of the Seismic Low Velocity and High Attenuation Zone in the Upper Mantle', *Earth Planet. Sci. Lett.* **157**, 193–207.

Key, K. and Constable, S.: 2002. 'Broadband Marine MT Exploration of the East Pacific Rise at 9°50'N', *Geophys. Res. Lett.*, **29**(22). doi:10.1029/2002GL016035.

Key, K. and Constable, S.: 2004, 'Constraining the Magmatic Budget of the EPR at 9°N Using Broadband Marine MT', *R.V. Roger Revelle Cruise Report*, p. 13.

Kohlstedt, D. L., and Mackwell, S. J.: 1998. 'Diffusion of Hydrogen and Intrinsic Point Defects in Olivine', *Z. Phys. Chem.* **207**, 147–162.

Koyama, T.: 2002. 'A Study of the Electrical Conductivity of the Mantle by Voltage Measurements for Submarine Cables', Ph.D. thesis, University of Tokyo.

Lilley, F.E.M., White, A., Heinson, G., and Procko, K.: 2004. 'Seeking a Seafloor Magnetic Signal from the Antarctic Circumpolar Current', *Geophys. J. Int.* **157**, 175–186. doi:10.1111/j.1365-246X. 2004.02174.x.

Lilley, F. E. M. T., White, A., and Heinson, G.: 2001. 'Earth's Magnetic Field: Ocean Current Contributions to Vertical Profiles in Deep Oceans', *Geophys. J. Int.* **147**, 163–175.

Lizarralde, D., Chave, A. D., Hirth, G., and Schultz, A.: 1995. 'Northeastern Pacific Mantle Conductivity Profile from Long-Period Magnetotelluric Sounding Using Hawaii-to-California Submarine Cable Data', *J. Geophys. Res.* **100**(B9), 17873–17854.

MacGregor, L.: 1999. 'Marine Controlled Source Electromagnetic Sounding: Development of a Regularised Inversion for 2-Dimensional Resistivity Structures', *LITHOS Science Report* **1**, 103–109.

MacGregor, L., Sinha, M., and Constable, S.: 2001. 'Electrical Resistivity Structure of the Valu Fa Ridge, Lau Basin, from Marine Controlled-Source Electromagnetic Sounding', *Geophys. J. Int.* **146**, 217–236.

MacGregor, L. M., Constable, S., and Sinha, M. C.: 1998. 'The RAMESSES Experiment – III. Controlled Source Electromagnetic Sounding of the Reykjanes Ridge at 57° 45′N', *Geophys. J. Int.* **135**, 773–789.

MacGregor, L. M., Greer, A. A., Sinha, M. C., and Peirce, C.: 2002. 'Properties of Crustal Fluids at the Valu Fa Ridge, Lau Basin, and Their Relationship to Active Hydrothermal Circulation, from Joint Analysis of Electromagnetic and Seismic Data', *LITHOS Science Report* **4**, 121–130.

Mainprice, D., Barruol, G., and Ben Ismaïl, W.: 2000. 'The Seismic Anisotropy of the Earth's Mantle: From Single Crystal to Polycrystal', in S. Karato, A. M. Forte, R. C. Liebermann, G. Masters, and L. Stixrude (eds.), *Earth's Deep Interior: Mineral Physics and Tomography: From the Atomic to the Global Scale, Vol. 117 of Geophys. Monogr.*, AGU, Washington, DC, pp. 237–264.

Nolasco, R., Tarits, P., Filloux, J. H. and Chave, A. D.: 1998. 'Magnetotelluric Imaging of the Society Islands Hotspot', *J. Geophys. Res.* **103**(B12), 30,287–30,309.

Oldenburg, D. W.: 1981. 'Conductivity Structure of Oceanic Upper Mantle Beneath the Pacific Plate', *Geophys. J.R. Astr. Soc.* **65**, 359–394.

Palshin, N. A.: 1996. 'Oceanic Electromagnetic Studies: A Review', *Surv. Geophys.* **17**, 455–491.

Park, C., Tamaki, K. and Kobayashi, K.: 1990. 'Age-depth Correlation of the Philippine Sea Back-arc Basins and other Marginal Basins in the World', *Tectonophysics* **181**, 351–371.

Park, J., Tsuru, T., Kodaira, S., Cummins, P.R. and Kaneda, Y.: 2002. 'Splay Fault Branching Along the Nankai Subduction Zone', *Science* **297**, 1157–1160.

Park, S.K. and Ducea, M.N.: 2003. 'Can In situ Measurements of Mantle Electrical Conductivity be Used to Infer Properties of Partial Melts?', *J. Geophys. Res.*, **108**(B5), doi:10. 1029/2002JB001899.

Price, A. T.: 1949. 'The Induction of Electric Currents in Non-uniform Thin-sheets and Shells', *Quart. J. Mech. App. Math.* **2**, 283–310.

Rodi, W., and Mackie, R. L.: 2001. 'Nonlinear Conjugate Gradients Algorithm for 2-D Magnetotelluric Inversion', *Geophysics* **66**(1), 174–187.

Schwalenberg, K., and Edwards, R. N.: 2004. 'The Effect of Seafloor Topography on Magnetotelluric Fields: An Analytical Formulation Confirmed with Numerical Results', *Geophys. J. Int.* **159**, 607–621. doi:10.1111/j.1365-246X.2004.02280.x.

Seama, N., Baba, K., Utada, H., Toh, H., Tada, N., Ichiki, M. and Matsuno, T.: 2004, '1D Electrical Conductivity Structure Beneath the Philippine Sea: Results from an Ocean Bottom Magnetotelluric Survey', *Phys. Earth Planet. Int.*, submitted.

Sinha, M. C., Constable, S. C., Peirce, C., White, A., Heinson, G., MacGregor, L. M., and Navin, D. A.: 1998. 'Magmatic Processes at Slow Spreading Ridges: Implication of the RAMESSES Experiment at 57° 45′N on the Mid-Atlantic Ridge', *Geophys. J. Int.* **135**, 731–745.

Siripunvaraporn, W., and Egbert, G.: 2000. 'An Efficient Data-Subspace Inversion Method for 2-D Magnetotelluric Data', *Geophysics* **65**(3), 791–803.

Smith, J. T., and Booker, J. R.: 1991. 'Rapid Inversion of Two- and Three-dimensional Magnetotelluric Data', *J. Geophys. Res.* **96**(B3), 3905–3922.

The MELT Seismic Team.: 1998. 'Imaging the Deep Seismic Structure Beneath a Mid-Ocean Ridge: The MELT Experiment', *Science* **280**, 1215–1218.

Tarits, P., Chave, A. D., and Schultz, A.: 1993. 'Comment on "The Electrical Conductivity of the Oceanic Upper Mantle" by G. Heinson and S. Constable', *Geophys. J. Int.* **114**, 711–716.

Toh, H.: 2003. 'Asymmetric Electrical Structures Beneath Mid-ocean Ridges', *J. Geography* **112**(5), 684–691(in Japanese).

Toh, H., Goto, T., and Hamano, Y.: 1998. 'A New Seafloor Electromagnetic Station with an Overhauser Magnetometer, a Magnetotelluric Variograph and an Acoustic Telemetry Modem', *Earth Planet. Space* **50**, 895–903.

Toh, H., Hamano, Y. and Goto, T.: 2001. 'Seafloor Electromagnetic Station: The Third Generation', in: *OHP/ION Joint Symposium Long-term Observations in the Oceans: Current Status and Perspectives for the Future*, pp. 21–23.

Toh, H., Hamano, Y., Ichiki, M., and Utada, H.: 2004. 'Geomagnetic Observatory Operates at the Seafloor in the Northwest Pacific Ocean', *EOS* **85**(45), 467–473.

Toomey, D. R., Wilcock, W. S. D., Solomon, S. C., Hammond, W. C., and Orcutt, J. A.: 1998. 'Mantle Seismic Structure Beneath the MELT Region of the East Pacific Rise from P and S Wave Tomography', *Science* **280**, 1224–1227.

Turcotte, D.L. and Schubert, G.: 2002. *Geodynamics*, 2nd ed., Cambridge University Press, Cambridge, UK.

Turner, I. M., Peirce, C., and Sinha, M.: 1999. 'Seismic Imaging of the Axial Region of the Valu Fa Ridge, Lau Basin – The Accretionary Processes of an Intermediate Back-arc Spreading Ridge', *Geophys. J. Int.* **138**, 495–519.

Uchida, T.: 1993. 'Smooth 2-D Inversion for Magnetotelluric Data Based on Statistical Criterion ABIC', *J. Geomag. Geoelectr.* **45**, 841–858.

Unsworth, M. J., Travis, B. J., and Chave, A. D.: 1993. 'Electromagnetic Induction by a Finite Electric Dipole Source Over a 2-D Earth', *Geophysics* **58**(2), 198–214.

Utada, H., Koyama, T., Shimizu, H. and Chave, A.D.: 2003. 'A Semi-Global Reference Model for Electrical Conductivity in the Mid-Mantle Beneath the North Pacific Region', *Geophys. Res. Lett.*, **30**(4), doi:10.1029/2002GL016092.

Wang, L., Zhang, Y. and Essene, E. J.: 1996. 'Diffusion of the Hydrous Component in Pyrope', *American Mineralogist* **81**, 706–718.

Wessel, P., and Smith, W. H. F.: 1998. 'New, Improved Version of the Generic Mapping Tools Released', *EOS Trans. AGU* **79**, 579.

Wolfe, C. J., and Solomon, S. C.: 1998. 'Shear-wave Splitting and Implications for Mantle Flow Beneath the MELT Region of the East Pacific Rise', *Science* **280**, 1230–1232.

Woods, S. C., Mackwell, S., and Dyar, D.: 2000. 'Hydrogen in Diopside: Diffusion Profiles', *Amer. Mineralogist* **85**, 480–487.

Woods, S.C. and Mackwell, S.J.: 1999. 'Hydrogen Diffusion in Enstatite', Technical Report Bayerisches Forschungsinstitut fur Experimentelle Geochemie und Geophysik, http://www.bgi.uni-bayreuth.de.

Xu, Y., Poe, B. T., Shankland, T. J., and Rubie, D. C.: 1998. 'Electrical Conductivity of Olivine, Wadsleyite, and Ringwoodite Under Upper-Mantle Conditions', *Science* **280**(29), 1415–1418.